Supplementary Information

Thermomechanically squeezed multi-mode phonon lasers with levitated optomechanics

Xintao Song[1,2], Guoyao Li[1,2], Tengfang Kuang[1,2], Ran Huang[3], Wei Xiong[1,2], Xinlin Chen[1,2], Xiang Han[1,2], Yang Zhang[1,2], Franco Nori[3,4], Hui Jing[5*], Hui Luo[1,2*], Guangzong Xiao[1,2*]

[1]College of Advanced Interdisciplinary Studies, National University of Defense Technology, Changsha, China

[2]Nanhu Laser Laboratory, National University of Defense Technology, Changsha, China

[3]Quantum Information Physics Theory Research Team, Center for Quantum Computing (RQC), RIKEN, Wakoshi, Saitama, Japan

[4]Physics Department, University of Michigan, Ann Arbor MI, USA

[5]Institute for Quantum Science and Technology, College of Science, National University of Defense Technology, Changsha, China

*jinghui@hunnu.edu.cn; luohui.luo@163.com; xiaoguangzong@nudt.edu.cn.

Supplementary Note 1. Mechanical Squeezing in Various Optomechanical Systems

Supplementary Table 1 shows the comparison of parameters in various optomechanical systems which are designed for mechanical squeezing. Unlike thermal-state squeezing or quantum squeezing based on ground-state cooling, we directly squeeze a coherent phonon source, demonstrating a squeezed nonlinear phonon laser.

Supplementary Table 1. Optomechanical systems for mechanical squeezing

Features	Ultrahigh-Q membrane[1]	Suspended Nano-string[2]	Nanosphere LOM system[3]	Microsphere LOM system
Phonon lasing	×	×	×	✓
Size of the oscillator	5 mm (lateral)	~ 100 nm	32 nm	2 μm
Mass of the oscillator	~ 10^{-9} kg	~ 10^{-18} kg	~ 10^{-19} kg	~ 10^{-14} kg
Optical gain	×	×	×	✓
Air pressure	~10^{-7} mbar	~10^{-4} mbar	~10^{-1} mbar	20 mbar
Squeezing degree	3 dB	3 dB	2.7 dB	3.15dB
Harmonics squeezing	×	×	×	✓

Notation: LOM system, levitated optomechanical system, ✓ for yes; × for no.

We note that our microsphere is two orders larger in size and five orders higher in mass than the nanosphere. In contrast to other phonon squeezing realizations, we have demonstrated efficient phonon squeezing in a phonon laser at a higher pressure (3 to 8 orders), enabled by the optical gain. Under a pressure of ~ 20 mbar, a maximum squeezing of 3.15 ± 0.35 dB is achieved for the fundamental mode.

Moreover, we confirm for the first time that not only the fundamental-mode phonon laser but also its nonlinear higher-order harmonics can be squeezed without the need of any complicated external feedback control techniques. This manipulation of higher-order harmonics establishes the foundation for parallel sensing protocols across multiple degrees of freedom.

In addition, the squeezing protocol in our work is different from the scheme of parametric amplification in the Suspended Nano-string system. In Ref. [2], a phase-locked system is employed to maintain the phase of the squeezing signal and the mechanical oscillator, as the squeezing generated by parametric amplification is phase-sensitive. In contrast, we employ the protocol of non-adiabatic frequency shifts to generate squeezing, which is inherently free from the 3 dB squeezing limit without the need of any complicated external feedback control techniques.

Supplementary Note 2. Theoretical Framework for Squeezing via Non-adiabatic Frequency Shifts

This appendix outlines the theoretical foundation for generating mechanical squeezing through non-adiabatic frequency shifts of phonon lasers. Here, we consider a phonon laser whose frequency switches periodically between Ω_1 and Ω_2 (where $\Omega_1 > \Omega_2$). The corresponding system Hamiltonians are given by:

$$\begin{aligned} \hat{H}_1 &= \frac{1}{2m}\hat{p}^2 + \frac{1}{2}m\Omega_1^2\hat{x}^2, \\ \hat{H}_2 &= \frac{1}{2m}\hat{p}^2 + \frac{1}{2}m\Omega_2^2\hat{x}^2, \end{aligned} \tag{1}$$

where m represents the mass of the mechanical oscillator. $\hat{p}$ and $\hat{x}$ denote the momentum and position operators, respectively. The annihilation operators for these modes are defined as

$$\begin{aligned} \hat{b}_1 &= \sqrt{\frac{m\Omega_1}{2\hbar}}\left(\hat{x} + \frac{i\hat{p}}{m\Omega_1}\right), \\ \hat{b}_2 &= \sqrt{\frac{m\Omega_2}{2\hbar}}\left(\hat{x} + \frac{i\hat{p}}{m\Omega_2}\right), \end{aligned} \tag{2}$$

which satisfies the standard commutation relation $[\hat{b}_i, \hat{b}_i^\dagger] = 1$ (i = 1,2). Before the squeezing operation ($t < 0$), the mechanical oscillator evolves under $\hat{H}_1$ with the mechanical frequency Ω_1. When the frequency of the mechanical oscillator is abruptly adjusted from Ω_1 to Ω_2 within a very short time scale ($\Delta t \ll 1/\Omega_1$), the Hamiltonian is switched from $\hat{H}_1$ to $\hat{H}_2$ instantaneously. Immediately after the sudden change, the wave function remains unchanged in real space. The momentum and position operators $\hat{p}$ and $\hat{x}$ in Supplementary Equation (2) can be eliminated. This is precisely the key condition that enables the theory to generate squeezing. Then the creation and annihilation operators $\hat{b}_2$ and $\hat{b}_2^\dagger$ can be easily calculated with the form of the Bogoliubov transformation:

$$\begin{aligned}\hat{b}_2 &= \alpha\hat{b}_1 + \beta\hat{b}_1^\dagger,\\ \hat{b}_2^\dagger &= \alpha^*\hat{b}_1^\dagger + \beta^*\hat{b}_1,\end{aligned} \tag{3}$$

where $\alpha = \frac{\Omega_1+\Omega_2}{2\sqrt{\Omega_1\Omega_2}}$ and $\beta = \frac{\Omega_1-\Omega_2}{2\sqrt{\Omega_1\Omega_2}}$ satisfy $\alpha^2-\beta^2=1$. Then we take $\alpha = \cosh(r)$ and $\beta = \sinh(r)e^{i\theta}$, Supplementary Equation (3) can be rewritten as:

$$\begin{aligned}\hat{b}_2^\dagger &= \cosh(r)\hat{b}_1^\dagger + \sinh(r)\hat{b}_1 e^{i\theta} = \hat{S}(r)\hat{b}_1^\dagger\hat{S}^\dagger(r),\\ \hat{b}_2 &= \cosh(r)\hat{b}_1 + \sinh(r)\hat{b}_1^\dagger e^{i\theta} = \hat{S}^\dagger(r)\hat{b}_1\hat{S}(r),\end{aligned} \tag{4}$$

where $\hat{S}(\xi) = \exp[(\xi^*\hat{b}_1^2 - \xi\hat{b}_1^{\dagger 2})/2]$ is the squeezing operator, $\xi = re^{i\theta}$ is the squeezing parameter, $r = \ln(\Omega_1/\Omega_2)/2$ is the squeezing magnitude, and θ is the squeezing angle. When $\Omega_2 < \Omega_1\,(\Omega_2 > \Omega_1)$, the position(momentum) is squeezed for

$$\begin{cases}\sinh(r) > 0, e^{i\theta} = 1 & \rightarrow \quad \frac{\theta}{2} = 0\\ \sinh(r) < 0, e^{i\theta} = -1 & \rightarrow \quad \frac{\theta}{2} = \frac{\pi}{2}\end{cases}. \tag{5}$$

After non-adiabatic frequency shifts, the squeezing degree is given by:

$$\lambda = -10\log_{10} e^{-r} = 5\log_{10}\frac{\Omega_1}{\Omega_2}. \tag{6}$$

In our squeezing protocol, each square-wave pulse generates two distinct squeezing events. During the pulse, the oscillator’s phase-space distribution rotates at Ω_2 continuously. At $t = \tau$, the frequency is instantaneously switched back to Ω_1. To find the net effect on the original $\hat{b}_1$ mode, we must map the final $\hat{b}_2(\tau)$ back to the $\hat{b}_1$ basis.

The full evolution of the quadrature vector $\vec{V}$ is described by a linear transformation

$$\vec{V}(\tau)=M\vec{V}(0), \tag{7}$$

where the symplectic matrix M admits decomposition:

$$\begin{aligned} M &= R(\theta)\cdot S(2r)\cdot R(\beta) \\ &= \begin{pmatrix} \cos\theta & \sin\theta \\ -\sin\theta & \cos\theta \end{pmatrix}\begin{pmatrix} e^{-2r} & 0 \\ 0 & e^{2r} \end{pmatrix}\begin{pmatrix} \cos\beta & \sin\beta \\ -\sin\beta & \cos\beta \end{pmatrix}. \end{aligned} \tag{8}$$

Here, $S(2r)$ is a squeezing matrix, and $R(\theta)$ is a rotation matrix. The angles θ and β depend on the evolution time τ and the frequencies Ω_1 and Ω_2.

The degree of squeezing is quantified by the minimum variance of a generalized quadrature, derived from the eigenvalues of the covariance matrix MM^{T}. The singular values of M determine the amplification and attenuation factors of the quadrature noise. Since $\det\left(MM^T\right)=1$, we can parametrize the eigenvalues of MM^T as (μ, $1/\mu$) for some parameter where $\mu > 0$. Note that $\sqrt{\mu}$ quantifies the deformation of the standard deviations of the rotated quadratures. The mechanical squeezing parameter thus reads (in decibels) $\lambda(\tau)=10\left|\log_{10}\left(\sqrt{\mu}\right)\right|$. When the system evolves for an integer number of a half-integer number of cycles, switching back to Ω_1 undoes the initial squeezing. Conversely, if the switch back to Ω_1 occurs after an odd number of quarter-periods, the squeezing magnitude doubles to $2r$, the degree of squeezing is expressed in decibels (dB):

$$\lambda_{\max}\left(\frac{\pi}{2\Omega_2}\right)=10\log_{10}\frac{\Omega_1}{\Omega_2}(\mathrm{dB}). \tag{9}$$

This result directly links the achievable noise reduction to the ratio of the two trapping frequencies.

Without loss of generality, the same frequency jump also applies to the second-harmonic mode. In our nonlinear phonon lasers, the fundamental (second-harmonic) frequency is locked to Ω_1 ($2\Omega_1$). When the fundamental frequency has a non-adiabatic change from Ω_1 to Ω_2, the second harmonic does so from $2\Omega_1$ to $2\Omega_2$. The frequency ratio $2\Omega_1/2\Omega_2 = \Omega_1/\Omega_2$ is the same as that of the fundamental mode, so the squeezing parameter $r = \ln(\Omega_1/\Omega_2)/2$ is identical for both modes.

Supplementary Note 3. Frequency-tunable Nonlinear Phonon Lasers

We systematically characterized three hallmark features: threshold behavior, linewidth narrowing, and coherence (via the normalized second-order correlation function $g^{(2)}(0)$). The results are summarized in Supplementary Fig. 1. As shown in Supplementary Figs. 1**a** and 1**b**, the linewidths of both modes narrow dramatically with the increasing of intracavity power, confirming threshold behavior. Notably, the second harmonic exhibits a broader linewidth than the fundamental mode, consistent with its lower mechanical quality factor. As shown in Supplementary Figs. 1**e** and 1**f**, $g^{(2)}(0)$ drops to near 1 and the phonon numbers increase markedly. These observations collectively confirm the three established hallmarks of a phonon-lasing state for both the fundamental and the second harmonic modes.

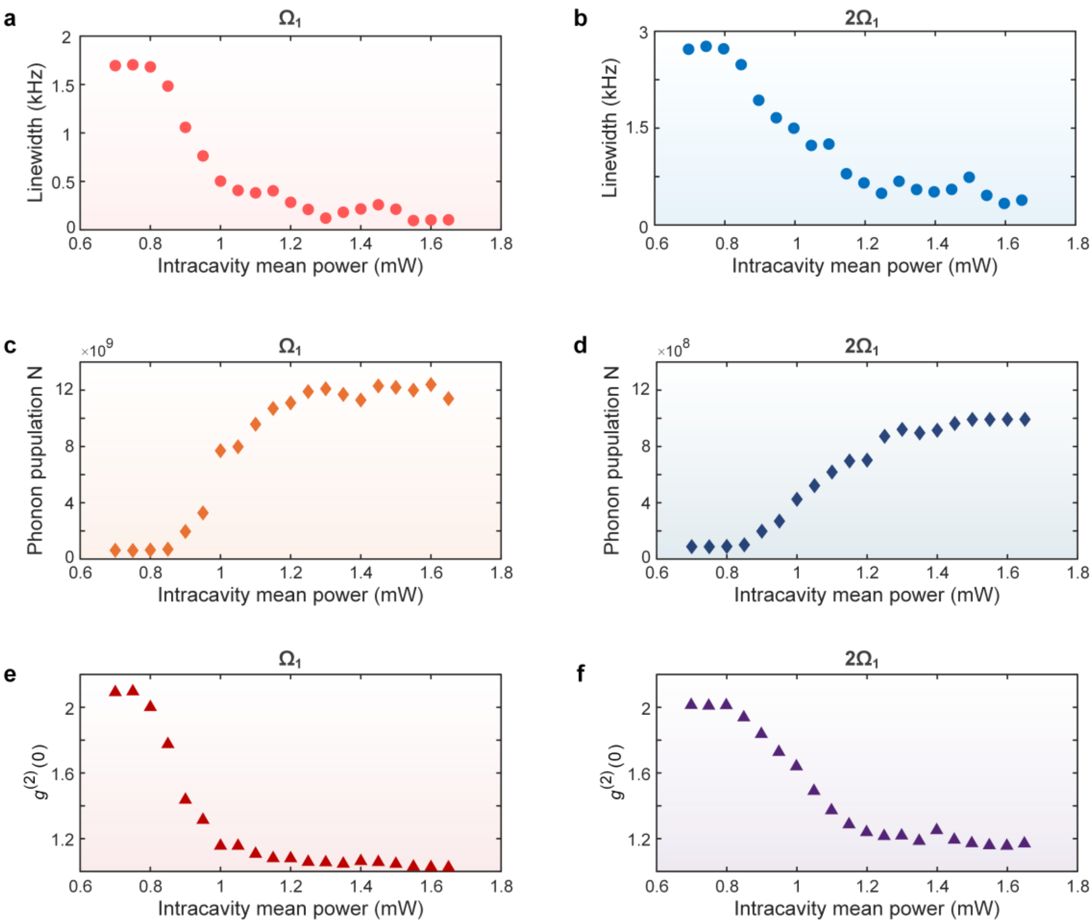

Supplementary Fig. 1. Characterization of phonon lasers for the fundamental mode (a, c, e) and the second harmonic mode (b, d, f). (a, b) Linewidth, (c, d) phonon population and the normalized second-order correlation function $g^{(2)}(0)$ (e, f) vary with the intracavity mean power.

Implementing the squeezing protocol via non-adiabatic frequency switching requires a tunable phonon laser frequency. To confirm this tunability, we varied the power of trapping beam, meanwhile the optical power in the active ring cavity holds 1.5 mW. This approach enabled continuous tuning of the frequency of nonlinear phonon laser, as illustrated in Supplementary Fig. 2.

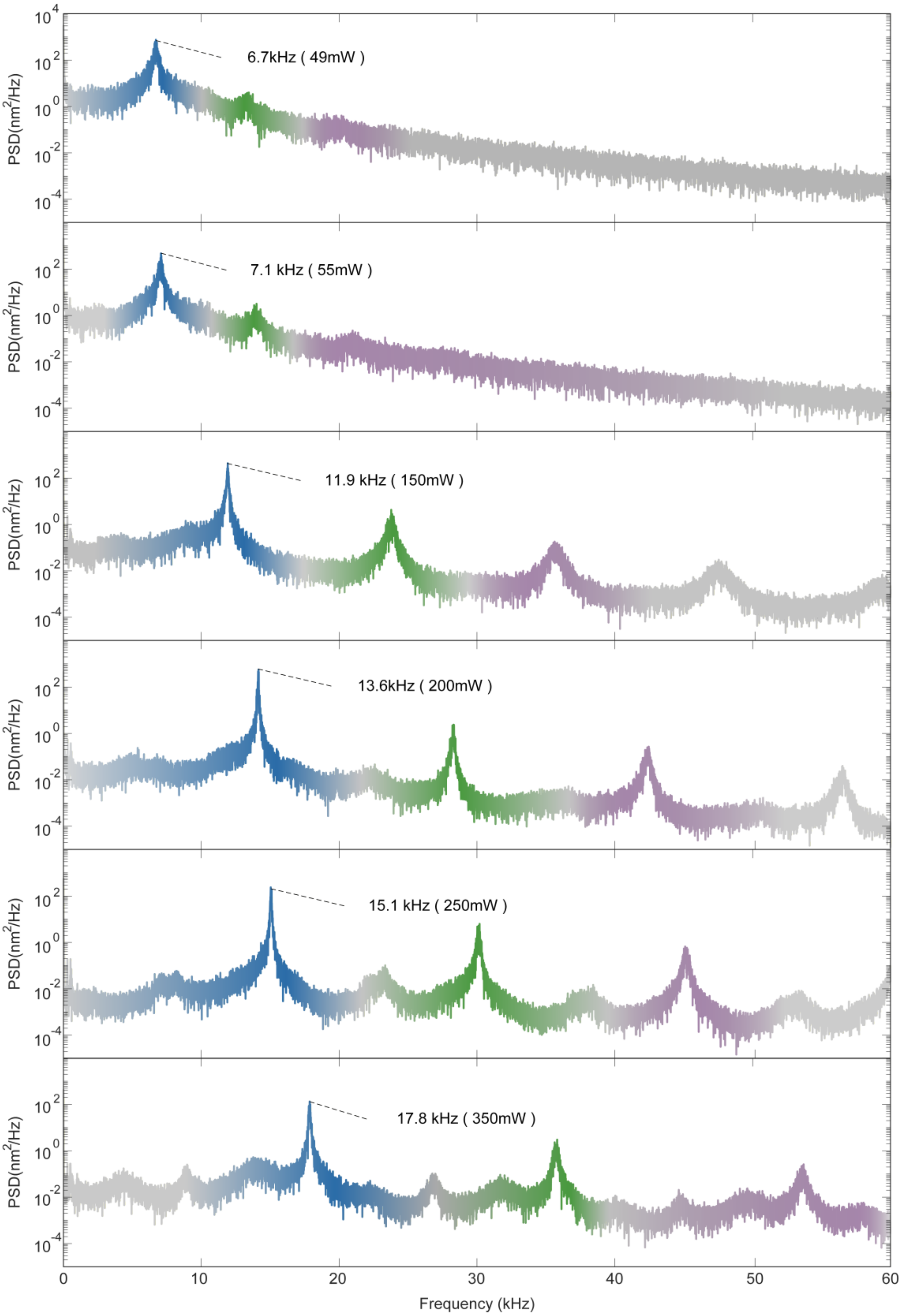

Supplementary Fig. 2. Frequency-tunable nonlinear phonon laser. The measured PSD of nonlinear phonon laser with different optical power.

We observed that the coherence of the phonon laser could not be well maintained as the trapping beam power decreased. As shown in Supplementary Fig. 3, a rapid growth in $g^{(2)}(0)$ is observed for trapping powers below 55mW, demonstrating a pronounced reduction in coherence. A similar behavior is also observed for the second harmonic mode, whose $g^{(2)}(0)$ increases as the trapping power decreases below a threshold. We attribute this result to the position shift of the microsphere during the pulse duration τ at excessively low P_2. Specifically, in the active levitated optomechanical system, a levitated microsphere is placed under the focal points of the objective (NA = 0.25), interacting with the active cavity through dissipative coupling. The dissipative optomechanical coupling strength depends on the relative separation between the center of the microsphere and the focal points of the objectives. In this case, reducing the trapping power P_2 causes the microsphere to drop under gravity, thereby increasing its relative distance from the focal points of the objectives and weakening the dissipative optomechanical coupling. As a direct consequence, this weakening of the dissipative coupling suppresses the mechanical gain essential for the phonon laser, which manifests as a significant degradation in coherence for both the fundamental and second harmonic modes.

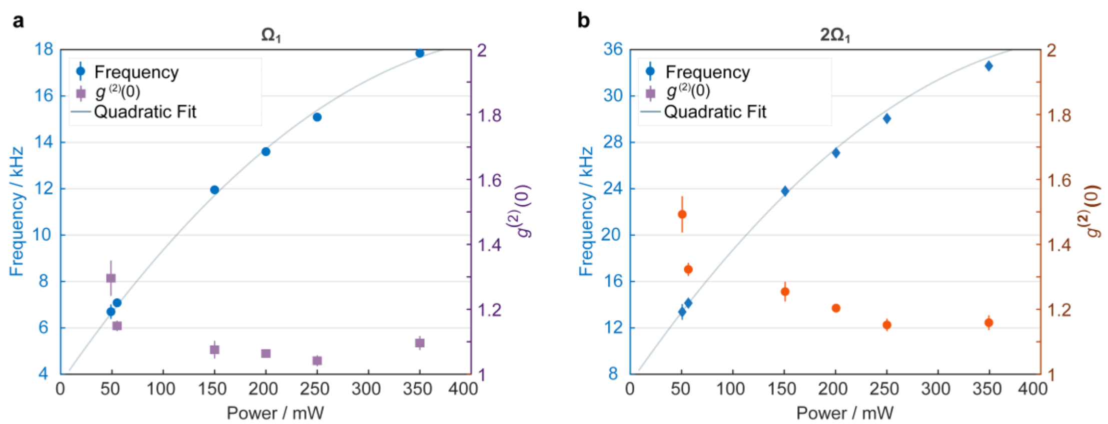

Supplementary Fig. 3. Fundamental and second harmonic mode frequencies of phonon lasers and their $g^{(2)}(0)$ as a function of the trapping power. a, The fundamental mode. **b,** The second harmonic mode. All error bars denote standard deviation.

Supplementary Note 4. Calculation of The squeezing degree

As depicted in Supplementary Fig. 4, we present the raw photodetector voltage trace in panel (a), which captures the real-time mechanical oscillation of the microsphere. Panel (b) shows the power spectral density (PSD) of the microsphere displacement under pulsed modulation. A series of equally spaced frequency comb teeth extending from low to high frequencies is clearly visible, originating from the square-wave modulation applied to the pump beam.

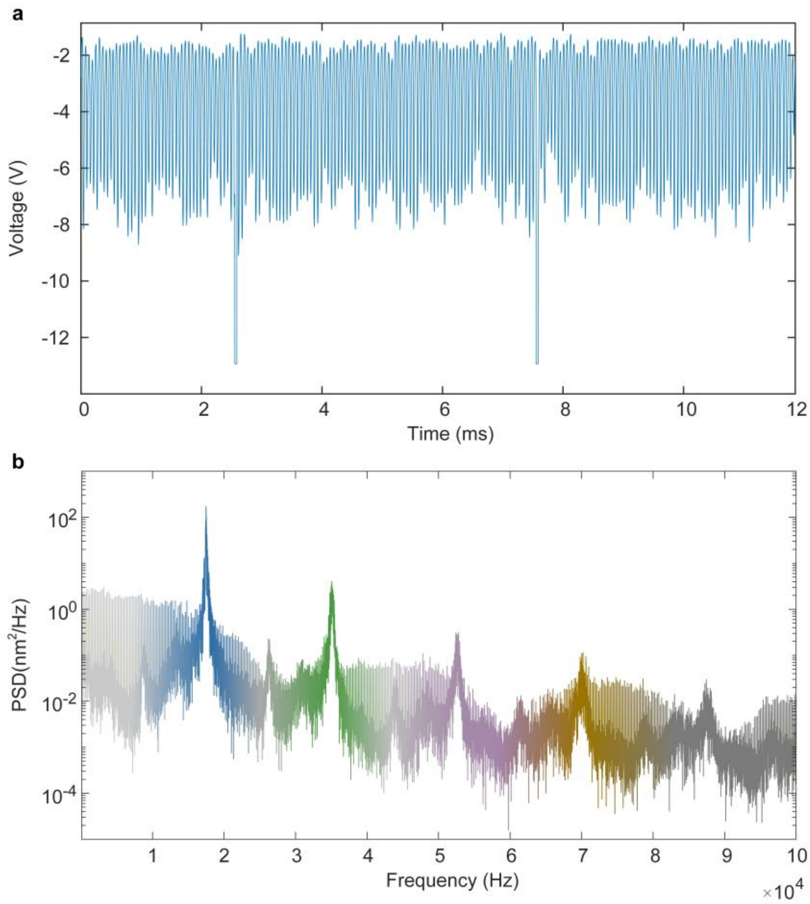

Supplementary Fig. 4. a, Raw photodetector voltage trace capturing the real-time mechanical oscillation of the microsphere. **b,** Power spectral density (PSD) of the microsphere displacement under pulsed modulation. The equally spaced frequency comb from low to high frequencies originates from the square-wave modulation of the pump beam.

The power spectral density (PSD) of the nonlinear phonon lasers shows that the original signal contains information about high-order mechanical harmonics and all three spatial degrees of freedom. As depicted in Supplementary Fig. 5, the residual peaks can be categorized into two types: 1) Modes from other spatial dimensions (y and z axes): The trapped microsphere possesses three translational degrees of freedom (x, y, z). In our experiment, the phonon lasing is primarily excited along the x-direction. Apart from this translation, the other spatial dimensions of the fundamental modes and the higher harmonics are crosstalk in the PSD. 2) Mechanical sidebands: When the system operates in the high-gain phonon lasing regime (especially at higher trapping power P_1), the stronger nonlinear optomechanical coupling leads to mechanical sidebands around the fundamental and harmonic modes. These mechanical sidebands become more pronounced when the nonlinearity is enhanced, which are indicated by the red boxes.

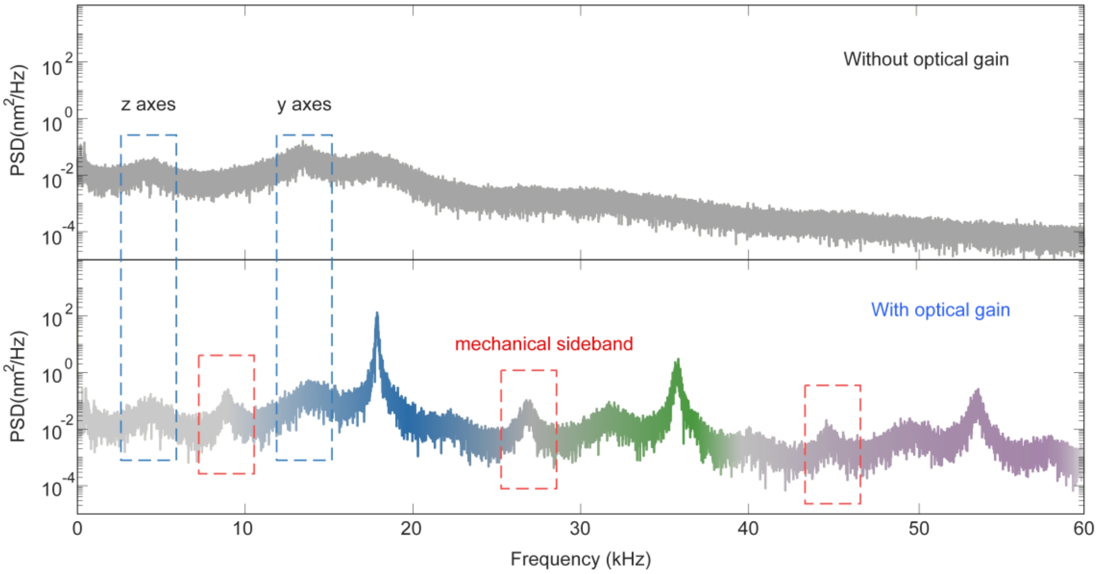

Supplementary Fig. 5. Power spectral density (PSD) of the trapped microsphere displacement. Top panel: Thermal state. Bottom panel: Phonon lasing. The blue boxes indicate residual peaks originating from the orthogonal y- axis and z-axis mechanical modes. The red boxes mark mechanical sidebands arising from stronger nonlinear optomechanical coupling in the lasing regime.

To analyze squeezing at the target frequency and spatial dimension (x axes), we applied a Butterworth bandpass filter to the original data, as it effectively removes harmonics at other frequencies. The filter parameters are given as follows: The filter order is 2, with a passband width of 2 kHz. As shown in Supplementary Fig. 6, this filter effectively isolates the target signal in the time domain.

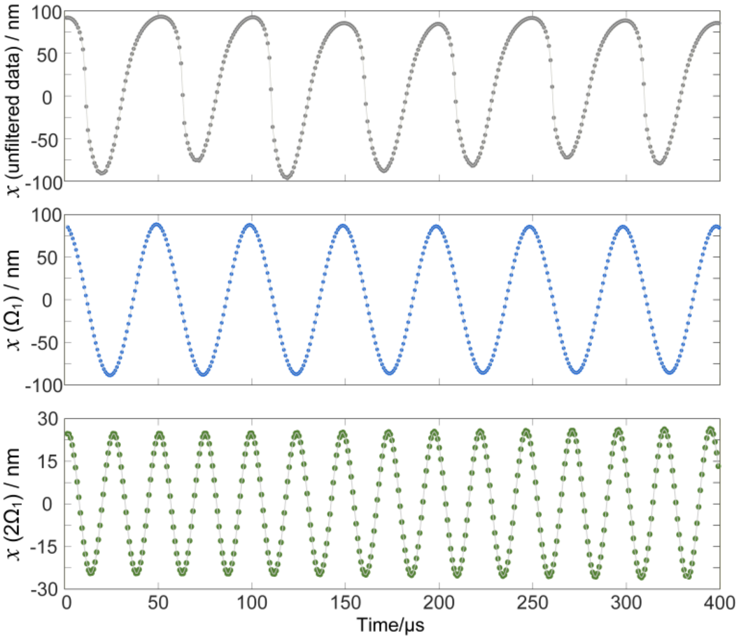

Supplementary Fig. 6. Filtering of a single time trace. Original time trace (grew). Filtered time trace (blue) using a bandpass filter near the fundamental frequency. Filtered time trace (green) using a bandpass filter near the second harmonic frequency.

To measure the degree of squeezing, we need to calculate the momentum noise variance of the phonon laser at a specific phase after (before) the pulse. However, the initial phase is uncertain at the time of pulse application. To overcome this, we repeatedly apply the squeezing pulse to construct the dynamical trajectories of phase space at time t. Supplementary Fig. 7**a** illustrates a schematic diagram of the computation process from dynamical trajectories to noise distribution in phase space. Based on the limit cycle identified in the phase space, we determine the amplitude A of the phonon laser from the expression $A\cos(\Omega_1 t)$, where A is the mean of $\sqrt{q_i^2 + p_i^2}$. For the fundamental mode, the squeezing parameter is $\xi = r \cdot e^{i\theta}$. When the pulse width $\tau = T_2/4$ (where $T_2 = 2\pi/\Omega_2$), the squeezing angle at the end of the pulse is $\pi/2$, i.e., the momentum quadrature is maximally squeezed. After the pulse, the phase-space distribution rotates at frequency Ω_1. Each point (q, p) in the dynamical trajectories corresponds to an ideal position $(q\cos\varphi, p\sin\varphi)$, allowing us to derive the noise deviation:

$$(\Delta q, \Delta p) = (q - A\cos\varphi, p - A\sin\varphi). \tag{10}$$

This deviation is then mapped into the noise distribution coordinate system as (q_{noise}, p_{noise} = $A+\Delta q$, $0+\Delta p$). In this case, we characterize the dynamical trajectories by a distribution of noise around the ideal trajectory in phase space. The corresponding Wigner Distributions takes an elliptical form, from which the squeezing angle is determined by the orientation of its minor axis, as shown in Supplementary Fig. 7**b**. Specifically, at a squeezing angle θ of 0, the position quadrature is squeezed while the momentum quadrature is anti-squeezed. The momentum noise variance is $\sigma_t^2 = \sum p_{noise}^2(t)$, and the degree of squeezing can be reliably calculated with the experimental data:

$$\lambda = 10\log_{10}\left(\frac{\sigma_0^2}{\sigma_t^2}\right)(dB), \tag{11}$$

where σ_0^2 and σ_t^2 denote the momentum noise variances of the initial state and the squeezed state at a specific phase after the pulse, respectively.

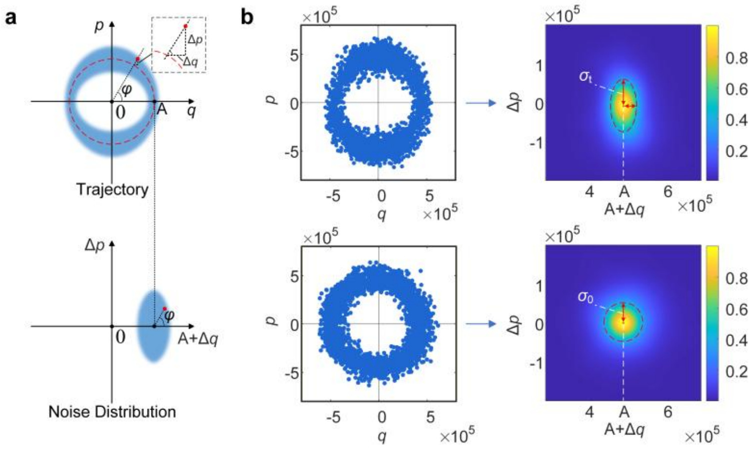

Supplementary Fig. 7. Dynamical trajectories and Wigner Distribution in phase space. a, Schematic diagram of the calculation from trajectory plots to noise distribution in phase space. **b**, The Winger Distribution of the phonon laser at time t is derived from the phase space data in the left panel, with a color bar indicating the normalized distribution density.

Supplementary Note 5. Error Analysis

To rule out the possibility that the observed squeezing arises from numerical differentiation noise, finite bandwidth, or detector noise, we perform two analyses.

First, under identical experimental conditions (same optical potential, data acquisition, and processing chain) but without applying the non-adiabatic frequency shifts, the system resides in a phonon-lasing state. With such, there is no squeezing. Applying the same numerical differentiation, bandpass filtering, and phase-space reconstruction to these reference data, the momentum noise variance ratio σ_t^2/σ_0^2 remains close to 1 (1.006271 ± 0.014093), indicating no observable noise reduction or amplification. This analysis confirms that our data processing doesn't artificially generate squeezing.

Second, we generate a pure sinusoidal signal (mimicking the coherent mechanical oscillation) and added Gaussian white noise to simulate the noise, achieving a signal-to-noise ratio of approximately 3 dB. This synthetic signal is no squeezing. We then apply it to the identical data processing pipeline (including numerical differentiation, bandpass filtering, and phase-space reconstruction). The results are shown in Supplementary Fig. 8. The reconstructed phase-space distribution exhibits a circular shape. The extracted momentum noise variance ratio remains close to 1 across all phases, demonstrating no artificial squeezing.

Taken together, these analyses provide strong evidence that the observed squeezing is a genuine physical effect and not an artefact of the data processing.

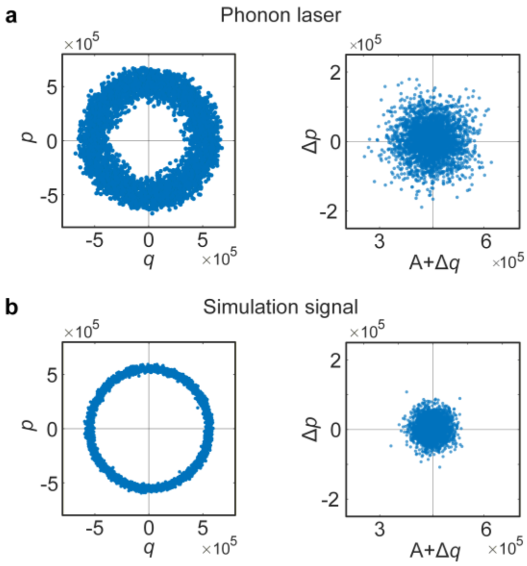

Supplementary Fig. 8. a, Phase-space distribution and quadrature noise of the phonon lasers. **b,** Phase-space distribution and quadrature noise of a synthetic reference signal. A pure coherent oscillation with added Gaussian white noise (SNR ≈ 3 dB).

Mass uncertainty. The squeezing degree is independent of the oscillator mass. While the absolute scales of q and p depend on the mass, both coordinates scale by the same factor $\sqrt{m}$. Therefore, the shape of the phase-space distribution (ellipticity, rotation angle, squeezing degree) remains unchanged. The certified microsphere (GBW12012b, SiO_2) has a value of 2.062 ± 0.02 μm. Using the density of SiO_2 (ρ = 2200 kg/m^3), the mass is 1.03×10^{-14} kg. The relative uncertainty in the radius is $\Delta R/R$ ≈ 0.97%, leading to a relative mass uncertainty:

$$\frac{\Delta m}{m} = 3\frac{\Delta R}{R} \approx 2.91\%. \tag{12}$$

The relative uncertainty in q and p is:

$$\frac{\Delta q}{q} = \frac{\Delta p}{p} = \frac{1}{2}\frac{\Delta m}{m} \approx 1.45\%. \tag{13}$$

Supplementary References

1. Patil, Y. S. et al. Thermomechanical Two-Mode Squeezing in an Ultrahigh-Q Membrane Resonator. *Phys. Rev. Lett.* **115**, 017202 (2015).
2. Huber, J. S. *et al.* Spectral Evidence of Squeezing of a Weakly Damped Driven Nanomechanical Mode. *Phys. Rev. X* **10**, 021066 (2020).
3. Rashid, M. *et al.* Experimental Realization of a Thermal Squeezed State of Levitated Optomechanics. *Phys. Rev. Lett.* **117**, 273601 (2016).